Letter

Fate of density waves in the presence of a higher-order van Hove singularity

Alkistis Zervou [1], Dmitry V. Efremov,[1,2] and Joseph J. Betouras [1]

[1]*Department of Physics and Centre for the Science of Materials, Loughborough University, Loughborough LE11 3TU, United Kingdom*
[2]*Leibniz Institute for Solid State and Materials Research Dresden, Helmholtzstrasse 20, D-01069 Dresden, Germany*

(Received 27 May 2022; revised 7 May 2023; accepted 19 September 2023; published 5 October 2023)

Topological transitions in electronic band structures, resulting in van Hove singularities in the density of states, can considerably affect various types of orderings in quantum materials. Regular topological transitions (of neck formation or collapse) lead to a logarithmic divergence of the electronic density of states (DOS) as a function of energy in two dimensions. In addition to the regular van Hove singularities, there are higher-order van Hove singularities (HOVHS) with a power-law divergence in DOS. By employing renormalization group techniques, we study the fate of a spin-density wave phase formed by nested parts of the Fermi surface, when a HOVHS appears in parallel. We find that the phase formation can be boosted by the presence of the singularity, with the critical temperature increasing by orders of magnitude, under certain conditions. We discuss possible applications of our findings to a range of quantum materials such as $Sr_3Ru_2O_7$, Sr_2RuO_4, and transition metal dichalcogenides.

DOI: 10.1103/PhysRevResearch.5.L042006

Introduction. Phase transitions, due to spontaneous symmetry breaking, with the emergence of an order parameter, are closely connected to specific features of the electronic band structure of itinerant systems. For example, various density waves appear in systems with nesting in the electronic band structure, i.e., the spectrum of the electronic excitations close to the Fermi level is characterized by $\varepsilon(\mathbf{p}+\mathbf{Q}) \approx -\varepsilon(\mathbf{p})$, where the vector $\mathbf{Q}$ is the nesting vector. Well-known representatives of density waves are the archetypal chromium [1], cuprates [2], iron pnictides [3,4], organics [5], and transition metal dichalcogenides [6]. Intriguingly, in a range of these materials the band structure hosts energetically close-by singularities in the density of states ν (DOS), which have been conjectured often to be crucial ingredients stabilizing the emergent phases [7–12].

Singularities and the associated divergence of DOS are a signature of the Fermi surface's topological transitions [13,14]. The two more well-known cases dealt with by Lifshitz [15] in his original work were the appearance or collapsing of a neck and the appearance or collapsing of a pocket in the Fermi surface. The former case was the ordinary van Hove singularity (VHS), with the Fermi surface locally consisting of a pair of intersecting straight lines. These two types of Fermi surface topological transitions have been observed along with their nontrivial consequences due to interactions in a wide range of quantum materials including cuprates, iron arsenic and ferromagnetic superconductors, cobaltates, Sr_2RuO_4, and heavy fermions [16–30].

However, higher-order van Hove singularities (HOVHS) display more exotic Fermi surface topological changes that lead to even more intriguing properties. They have been associated with exotic phenomena such as the nontrivial magnetic and thermodynamic properties in $Sr_3Ru_2O_7$ [13], correlated electron phenomena in twisted bilayer graphene near half filling [31], the so-called supermetal with diverging susceptibilities in the absence of long range order [32], and unusual Landau level structure in gated bilayer graphene [14]. Recently, a classification scheme for Fermi surface topological transitions and their associated DOS divergence was developed [33,34], as well as a method to detect and analyze them [35], while the effects of disorder were also studied [36].

Here, we study the general question about the fate of a spin-density wave (SDW) or a current charge-density wave (CDW), that is formed due to nesting of two parts of the Fermi surface when the Fermi energy is tuned so that a Fermi surface topological transition with HOVHS in the DOS at nearly the Fermi level emerges. If the degree of nesting is not significantly changed due to the HOVHS, the density wave phase, as naively expected, can be suppressed. Surprisingly, we find that it can get boosted, depending on the strength of the bare couplings in the Hamiltonian.

Model. We take three patches within the first Brillouin zone (BZ). Two of them (patches 1 and 2), with DOS ν_0 per spin, are nested both in the presence and absence of patch 3, which is the one associated with the singular DOS. The dispersion relations are $\varepsilon_1(\mathbf{k}) = -\varepsilon_2(\mathbf{k}+\mathbf{Q}) = v_F(k_x - k_F)$, where v_F is the Fermi velocity and k_F is the Fermi momentum of the two nested patches. The dispersion relation of the third patch with respect to the chemical potential μ is modeled by $\varepsilon_3(\mathbf{k}) = \alpha k^2 + \gamma(k_x^4 + k_y^4 - 6k_x^2k_y^2) - \mu$. In the present work we consider the problem at the quantum critical point assuming $\alpha = 0$ for simplicity. This is the form that has been recently considered for a HOVHS in $Sr_3Ru_2O_7$ [13]. The

resulting DOS per spin for patch 3 is then

$$\nu(\varepsilon) = A_4|\varepsilon|^{-1/2}, \tag{1}$$

where $A_4 = \alpha_4/\sqrt{\gamma}$ with $\alpha_4 = \frac{1}{16}\frac{1}{\pi^{3/2}}\frac{\Gamma(\frac{1}{4})}{\Gamma(\frac{3}{4})} \approx 0.033$, Γ is the gamma function, and γ is measured in units of $1/\nu_0$. Below, we take $1/\gamma = 100\nu_0$. We consider all possible short-range electron-electron interactions allowed by symmetry and obeying the conservation of momenta. We assume $\mathbf{Q}$ to be incommensurate, as such Umklapp processes are not relevant. Taking into account all possible *relevant* two-particle interactions involving fermions in the three patches, the effective Hamiltonian reads

$$\begin{aligned}\mathcal{H} = &\int d\mathbf{k} \sum_{\sigma=\uparrow,\downarrow}\sum_{a=1,2,3} \varepsilon_a(\mathbf{k}) c^\dagger_{a\sigma}(\mathbf{k}) c_{a\sigma}(\mathbf{k}) + \bar{g}_1 \int \{d\mathbf{k}_i\} \sum_{\sigma\sigma'} c^\dagger_{1\sigma}(\mathbf{k}_1) c^\dagger_{2\sigma'}(\mathbf{k}_2) c_{2\sigma'}(\mathbf{k}_3) c_{1\sigma}(\mathbf{k}_4) \\ &+ \bar{g}_2 \int \{d\mathbf{k}_i\} \sum_{\sigma\sigma'} c^\dagger_{1\sigma}(\mathbf{k}_1) c^\dagger_{2\sigma'}(\mathbf{k}_2) c_{1\sigma'}(\mathbf{k}_3) c_{2\sigma}(\mathbf{k}_4) + \bar{g}_3 \int \{d\mathbf{k}_i\} \sum_{\sigma\sigma'} c^\dagger_{1\sigma}(\mathbf{k}_1) c^\dagger_{2\sigma'}(\mathbf{k}_2) c_{3\sigma'}(\mathbf{k}_3) c_{3\sigma}(\mathbf{k}_4) \\ &+ \bar{g}_4 \int \{d\mathbf{k}_i\} \sum_{\sigma\sigma'} c^\dagger_{3\sigma}(\mathbf{k}_1) c^\dagger_{3\sigma'}(\mathbf{k}_2) c_{3\sigma'}(\mathbf{k}_3) c_{3\sigma}(\mathbf{k}_4) + \bar{g}_5 \int \{d\mathbf{k}_i\} \sum_{\sigma\sigma',a=1,2} c^\dagger_{a\sigma}(\mathbf{k}_1) c^\dagger_{3\sigma'}(\mathbf{k}_2) c_{3\sigma'}(\mathbf{k}_3) c_{a\sigma}(\mathbf{k}_4) \\ &+ \bar{g}_6 \int \{d\mathbf{k}_i\} \sum_{\sigma\sigma',a=1,2} c^\dagger_{3\sigma}(\mathbf{k}_1) c^\dagger_{a\sigma'}(\mathbf{k}_2) c_{3\sigma'}(\mathbf{k}_3) c_{a\sigma}(\mathbf{k}_4) + \text{H.c.}, \end{aligned} \tag{2}$$

where a labels the patches; σ, σ' are spin indices; and patches 1 and 2 are the nested ones and are taken as equivalent. The $\bar{g}_1$ term describes density-density interactions between patches 1 and 2, $\bar{g}_2$ takes into account exchange interactions between patches 1 and 2, $\bar{g}_3$ describes pair transfer between patch 3 and patches 1 and 2, while $\bar{g}_4$ describes density-density within patch 3 and $\bar{g}_5$ and $\bar{g}_6$ density-density and exchange interactions, respectively, between patch 3 and each of patches 1 and 2 (Fig. 1). The interactions which are solely within patch 1 or patch 2 are irrelevant and are not presented in the Hamiltonian as the particle-particle and particle-hole bubbles associated with them are small and can be neglected in a parquet renormalization group (pRG). The conservation of momentum is assumed. In principle, the effective Hamiltonian and the relative strength of the interactions can be obtained starting with a short-range interaction (Hubard and Hund's model), when the orbitals that play a dominant role at each patch are known. We leave the parameters quite general to account for different possibilities. In the following, we use dimensionless g_i's with $g_i = \nu_0\bar{g}_i$.

Particle-particle and particle-hole bubbles. As the geometry of the system dictates, there are two characteristic momenta. The first one is the nesting vectors $\mathbf{Q}$, which connect patch 1 with patch 2. The second one $\tilde{\mathbf{Q}}$ connects patch 1 with patch 3 and patch 2 with patch 3. In the following, we denote by Π the particle-hole and by C the particle-particle noninteracting susceptibilities, respectively. The particle-hole susceptibility for patches 1 and 2 is $\Pi^{(12)}_{ph}(\omega = 0, \mathbf{Q}) = T\sum_n \int d\mathbf{k} G_1(\omega_n, \mathbf{k}) G_2(\omega_n, \mathbf{Q} + \mathbf{k})$, where $G_{1,2}(\omega_n, \mathbf{k}) = [i\omega_n - \varepsilon_{1,2}(\mathbf{k})]^{-1}$ are the corresponding Green's functions. Similarly, for the particle-particle bubble $C^{(12)}_{pp}(\omega = 0, \mathbf{q} = 0) = T\sum_n \int d\mathbf{k} G_1(\omega_n, \mathbf{k}) G_2(-\omega_n, -\mathbf{k})$. In the renormalization group (RG) process, the energy integration over the regions $[\varepsilon - \delta\varepsilon, \varepsilon]$ and $[-\varepsilon, -\varepsilon + \delta\varepsilon]$ results in

$$-\delta\Pi^{(12)}(\varepsilon, \mathbf{Q}) = \delta C^{(12)}(\varepsilon, q = 0) = \nu_0 \frac{\tanh\left(\frac{\varepsilon}{2T}\right)}{\varepsilon}\delta\varepsilon. \tag{3}$$

For patch 3 the leading divergences of free-particle susceptibilities are associated with the particle-particle $C^{(33)}$ and particle-hole $\Pi^{(33)}$ bubbles at zero momentum transfer. More specifically, the energy integration over the regions $[\varepsilon - \delta\varepsilon, \varepsilon]$ and $[-\varepsilon, -\varepsilon + \delta\varepsilon]$ leads to [37]

$$\delta\Pi^{(33)}(\varepsilon, q = 0) = -\frac{\nu(\varepsilon)}{2T}\cosh^{-2}\frac{\varepsilon}{2T}\delta\varepsilon, \tag{4}$$

$$\delta C^{(33)}(\varepsilon, q = 0) = \nu(\varepsilon)\frac{\tanh\left(\frac{\varepsilon}{2T}\right)}{\varepsilon}\delta\varepsilon, \tag{5}$$

where $\nu(\varepsilon)$ is given by Eq. (1). Comparing Eqs. (3)–(5), we see three different energy dependencies of the susceptibilities. At large energies $\varepsilon \gg T$ the slope of the susceptibilities in particle-particle and particle-hole channels for patches 1 and 2 are slowly decaying functions of ε as $-\delta\Pi^{(12)}/\delta\varepsilon = \delta C^{(12)}/\delta\varepsilon \sim 1/\varepsilon$, which leads to the standard ultraviolet $\log(\Lambda)$ and infrared $\log(\varepsilon)$ divergences. In contrast, the susceptibilities for patch 3 decay much faster with ε as $\delta C^{(33)}/\delta\varepsilon \sim \varepsilon^{-3/2}$ and $\delta\Pi^{(33)}/\delta\varepsilon \sim -\exp(-\varepsilon/T)/(T\sqrt{\varepsilon})$ when $\varepsilon \geqslant T$. If $\varepsilon < T$ then $\delta C^{(33)}/\delta\varepsilon$ and $\delta\Pi^{(33)}/\delta\varepsilon$ scale as $1/(T\sqrt{\varepsilon})$ with opposite sign. The divergence at the lower limit is removed by the temperature factor in the case of the particle-particle channels and it is completely absent in the case of the particle-hole channel. We have also checked

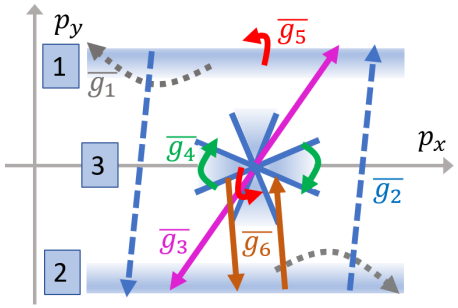

FIG. 1. Schematically, the interactions of the Hamiltonian Eq. (2).

the contribution of the susceptibilities $C^{(13)}(\mathbf{Q}-\tilde{\mathbf{Q}})$, $\Pi^{(13)}(\mathbf{Q}-\tilde{\mathbf{Q}})$ (similarly $C^{(23)}$ and $\Pi^{(23)}$) and found them to be negligible in comparison to $\Pi^{(12)}, C^{(12)}, \Pi^{(33)}, C^{(33)}$. Therefore, in the next we do not include them. This simplification allows us to work in energy space.

pRG equations. We employ one loop pRG, which can be connected to a functional RG (e.g., Ref. [11]) and has been used successfully, e.g., Refs. [10,38–41]. However, a cutoff scheme is needed for implementation of the procedure. In this work we use energy shell RG and the cutoff scheme is

$$\frac{1}{i\omega_n - \varepsilon(k)} \to \frac{\Theta(|\varepsilon(k)| - \Lambda)}{i\omega_n - \varepsilon(k)},$$

which interpolates between the zero propagator and the bare propagator as the cutoff Λ changes between 0 and ∞, whereby one obtains the energy shell pRG.

For the RG equations we only include the terms with the most diverging susceptibilities and redefine the RG flow parameter $L = \log(\frac{\Omega}{\Lambda})$, where $\Omega = 1/\nu_0$ is the bandwidth of pockets 1 and 2. The resulting set of differential equations has the following form:

$$\begin{aligned}
\dot{g_1} &= \eta_1 g_1^2 - \eta_2 g_3^2 + 2\eta_3 g_5(g_6 - g_5)\\
\dot{g_2} &= 2\eta_1\left(g_1 g_2 - g_2^2\right) - \eta_2 g_3^2 + \eta_3 g_6^2\\
\dot{g_3} &= -\eta_2 g_3 g_4\\
\dot{g_4} &= (\eta_3 - \eta_2) g_4^2\\
\dot{g_5} &= \eta_3 g_4(g_6 - g_5)\\
\dot{g_6} &= \eta_3 g_6 g_4
\end{aligned} \tag{6}$$

with

$$\eta_1 = \tanh\left(\frac{e^{-L}}{2\nu_0 T}\right) \tag{7}$$

$$\eta_2 = \frac{\alpha_4}{(\nu_0\gamma)^{1/2}} e^{L/2} \tanh\left(\frac{e^{-L}}{2\nu_0 T}\right) \tag{8}$$

$$\eta_3 = \frac{\alpha_4}{(\nu_0\gamma)^{1/2}} e^{-L/2} \frac{1}{2(\nu_0 T)\cosh^2\left(\frac{e^{-L}}{2\nu_0 T}\right)}. \tag{9}$$

The functions $\eta_{1,2,3}$ determine the low-energy cutoffs at T, for all bubbles $\Pi^{(12)}$, $C^{(12)}$, $\Pi^{(33)}$, and $C^{(33)}$.

pRG analysis. To understand the effect of the singularity, we compare the flow of g_1 and g_2, which are responsible for the formation of DWs, without and in the presence of patch 3. First we consider patches 1 and 2 without patch 3. Considering for simplicity $T \to 0$, the expression $\tanh(\frac{\epsilon}{2T}) \to 1$ and

$$\dot{g}_1 = g_1^2, \quad \dot{g}_2 = 2\left(g_1 g_2 - g_2^2\right). \tag{10}$$

The solution of system Eq. (10) is

$$\begin{aligned}
g_1 &= \frac{g_1^0}{1 - g_1^0 L},\\
g_2 &= \frac{1}{2}\frac{g_1^0}{1 - g_1^0 L} + \frac{1}{2}\frac{u^0}{1 + u^0 L},
\end{aligned} \tag{11}$$

where $u^0 = 2g_2^0 - g_1^0$ and $g_{1,2}^0$ are the bare values (initial conditions) of $g_{1,2}$. Following Ref. [38], the SDW and CDW vertices read

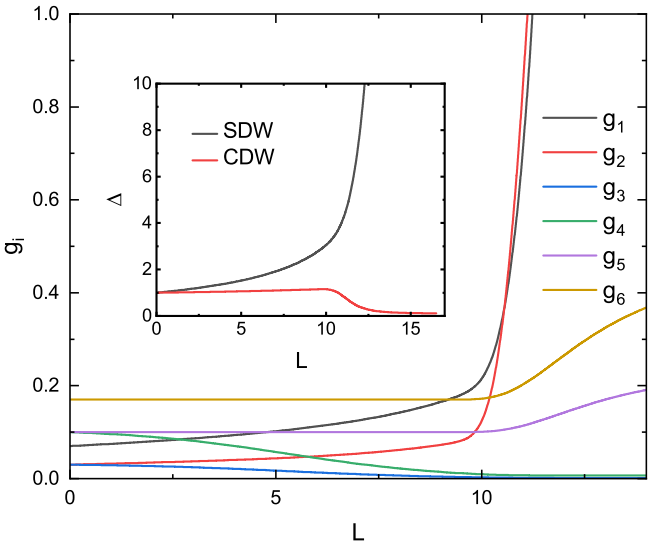

FIG. 2. The flow of g_i's in the presence of patch 3, for initial values $g_1^0 = 0.07$, $g_2^0 = 0.03$, $g_3^0 = 0.03$, $g_4^0 = 0.1$, $g_5^0 = 0.1$, and $g_6^0 = 0.17$ at $T = T_c$. The critical temperature for the SDW formation is found now at $T_c \propto 10^{-5}$, two orders of magnitude higher than in the absence of patch 3, where $T_c \propto 10^{-7}$. In the inset, Δ denotes Δ_{SDW} or Δ_{CDW} as calculated from Eq. (12).

$$\begin{aligned}
\Gamma_{\mathrm{SDW}} &= g_1(L) = \frac{g_1^0}{1 - g_1^0 L}\\
\Gamma_{\mathrm{CDW}} &= g_1 - 2g_2 = -\frac{u^0}{1 + u^0 L}.
\end{aligned} \tag{12}$$

The equations of the gap functions then are

$$\frac{d\Delta_\lambda}{dL} = \Gamma_\lambda \Delta_\lambda, \tag{13}$$

where λ = SDW or CDW, with solutions in the absence of patch 3:

$$\Delta_{\mathrm{SDW}} = \frac{\Delta_{\mathrm{SDW}}^0}{1 - g_1^0 L} \text{ and } \Delta_{\mathrm{CDW}} = \frac{\Delta_{\mathrm{CDW}}^0}{1 + u^0 L}.$$

The important point is that there are two independent channels leading to SDW and CDW order parameters. SDW is formed when the critical $L \to 1/g_1^0$, while CDW is formed when $L \to -1/u^0$. The presence of patch 3 renormalizes strongly these critical values at finite temperature.

Returning to the full set of the flow equations Eqs. (6) to investigate the effect of patch 3, we calculate the critical temperature in the presence and absence of patch 3. The critical temperature is defined as the temperature of the divergence of Δ_{CDW} or Δ_{SDW}. We fix the bare $g_1^0 = 0.07$ and $g_2^0 = 0.03$ and vary the remaining bare coupling constants. The results are presented in Figs. 2 and 3. The critical temperature in the absence of patch 3 is $T_c \approx 7 \times 10^{-7}$ (the flow of g_1, g_2 and the vertices are presented in the Supplemental Material [37]). When patch 3 is present, then the rest of the g_i's come into play. For the same initial values as before for g_1 and g_2 and for the same set of initial values of $g_4 = 0.1$, $g_5 = 0.1$, $g_6 = 0.17$, we present the behavior of the vertices for two

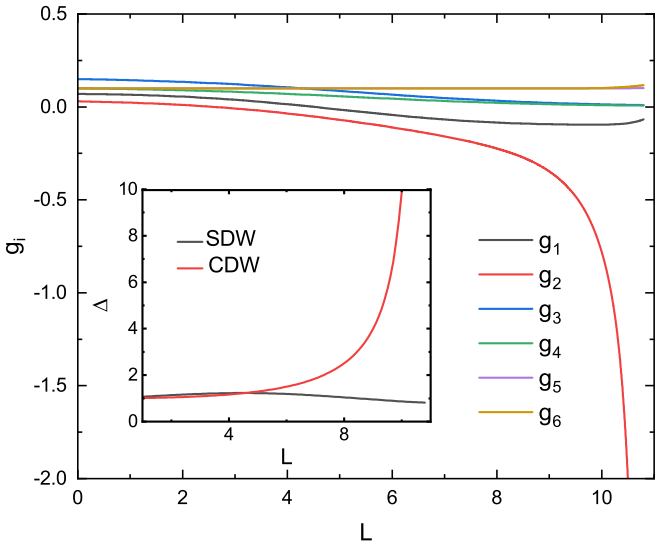

FIG. 3. The flow of g_i's in the presence of patch 3 for the same initial values as in Fig. 2 for all g_i^0 except from g_3^0, which is now $g_3^0 = 0.15$ at $T = T_c$. The critical temperature now corresponds to the transitions to CDW and is $T_c \propto 10^{-5}$.

cases, $g_3^0 = 0.03$ (Fig. 2) and $g_3^0 = 0.15$ (Fig. 3). In Fig. 2 the T_c of SDW is boosted by two orders of magnitude to $T_c = 4.1 \times 10^{-5}$, while in Fig. 3 the larger g_3^0 promotes the formation of CDW, with T_c again two orders of magnitude greater than the T_c of SDW without patch 3. As is evident, the presence of the singularity, with nonzero g_i's for $i = 3, 4, 5, 6$, renormalizes strongly g_1 and g_2. Depending on the initial conditions, the effect of the singular patch 3 on the DWs is summarized by the following statements: for small values, as physically expected, of the pair-transfer g_3^0 (i) the SDW is destroyed when $g_5^0 > g_6^0$, and (ii) if $g_5^0 < g_6^0$ it is very much enhanced (with T_c enhanced by potentially orders of magnitude). Otherwise, larger values of g_3^0 promote the formation of current CDW. A full investigation of parameters, in momentum space, will be presented elsewhere.

In the absence of patch 3, the flow equations Eqs. (6) are such that the repulsive interactions cannot be reverted to attractive. It is easy to see that in this case g_1 can only grow, while g_2 cannot change the sign. The presence of patch 3 makes it possible for g_1 and g_2 to change signs and become negative (attractive) [37], due to the overscreening effect caused by the HOVHS [38,40,42]. This is a very interesting feature of the model. For lower temperatures we searched for the possibility g_1 and/or g_2 to diverge (signature of superconducting instability), but we concluded that, at low temperature, this is not possible for this model.

Discussion. In this study we have considered the effect of a HOVHS on the formation of a density wave (in particular SDW) due to nesting of other parts of the FS. The scattering through the patch with the singular DOS can have very important consequences, depending on the bare values of the interactions. It can definitely destroy the phase, but surprisingly, it can also amplify the formation of the density wave and increase the corresponding T_c by orders of magnitude. The boosting of the DW formation happens as long as the exchange interactions between patch 3 and each of the nested patches is greater than the corresponding density-density interactions. In the opposite case, the SDW gets destroyed. We also find that if the initial value of the pair transfer between patch 3 and the other two patches is strong enough, a SDW can be turned to a current CDW. The different bare values of the interaction mimics material-specific effects such as the specific geometry in the BZ of the patches and the orbitals involved, which can be different in nature. One major question is the feasibility of stronger exchange interactions in comparison to density-density ones. This is possible in multiorbital systems [12,43].

Recently, many surprising experimental results of $Sr_3Ru_2O_7$ [44] were explained assuming the presence of a HOVHS in a magnetic field [13]. The reason that SDW phases (A and B) [45] only appear adjacent to a HOVHS by tuning the external magnetic field, although the same nesting vector connects the edges of the γ bands as well as other parts of the FS which respond less drastically to the magnetic field, was not explained. Although the difference of the present general theory to the experiments on $Sr_3Ru_2O_7$ is that the latter is a case of SU(2) symmetry breaking as HOVHS appears when the minority spins in the γ bands sink below Fermi energy, the present work can explain in principle why the SDW was detected only when the HOVHS appeared. Indeed, there are parts of the FS that can provide the nesting which are almost insensitive to the applied magnetic field while the γ bands are strongly affected. These bands are responsible for the formation of the HOVHS, which in turn can boost the formation of the SDW to a critical temperature that is measurable. Therefore, the mechanism presented here can be the key one to explain the SDW formation through the effect of the singularity at the center of the γ bands to the other nested pieces of the BZ. Also importantly, the existence of an SDW in Sr_2RuO_4 when it is strained and transverses a VHS has been established [46,47]. Our work could be relevant to this finding, but further work is needed.

Our theory could also explain, in principle, the CDW formation in 1T-VSe_2 [48,49] where a VHS is present [50] and a HOVHS at the Γ point of the BZ is seen in discrete Fourier transform (DFT) calculations [51]. This geometry corresponds to a dispersion relation with a term $\propto k^6 \cos(6\phi)$ that can boost the formation of the CDW. The difference is that the initial setup of the problem should favor a CDW instead of a SDW formation. We expect this theory to apply to many different materials in similar situations.

Acknowledgments. We thank Anirudh Chandrasekaran, Claudio Chamon, Clifford Hicks, and Ioannis Rousochatzakis for helpful discussions and, especially, Andrey Chubukov and Frank Kruger for a critical reading of the manuscript. We acknowledge the contribution of Garry Goldstein in the early stages of the work. The work was supported by EPSRC Grants No. EP/P002811/1 and No. EP/T034351/1 (J.J.B.). D.E. acknowledges partial financial support from DFG through the Project No. 449494427 and the Volkswagen Foundation through project "Synthesis, theoretical examination, and experimental investigation of emergent iron-based superconductors."

[1] E. Fawcett, Spin-density-wave antiferromagnetism in chromium, Rev. Mod. Phys. **60**, 209 (1988).

[2] W. D. Wise, M. C. Boyer, K. Chatterjee, T. Kondo, T. Takeuchi, H. Ikuta, Y. Wang, and E. W. Hudson, Charge-density-wave origin of cuprate checkerboard visualized by scanning tunnelling microscopy, Nat. Phys. **4**, 696 (2008).

[3] I. I. Mazin, D. J. Singh, M. D. Johannes, and M. H. Du, Unconventional superconductivity with a sign reversal in the order parameter of $LaFeAsO_{1-x}F_x$, Phys. Rev. Lett. **101**, 057003 (2008).

[4] P. Dai, J. Hu, and E. Dagotto, Magnetism and its microscopic origin in iron-based high-temperature superconductors, Nat. Phys. **8**, 709 (2012).

[5] P. Monceau, Electronic crystals: An experimental overview, Adv. Phys. **61**, 325 (2012).

[6] A. M. Gabovich, A. I. Voitenko, and M. Ausloos, Charge- and spin-density waves in existing superconductors: Competition between Cooper pairing and Peierls or excitonic instabilities, Phys. Rep. **367**, 583 (2002).

[7] L. van Hove, The occurrence of singularities in the elastic frequency distribution of a crystal, Phys. Rev. **89**, 1189 (1953).

[8] K. Kim, S. Kim, J. S. Kim, H. Kim, J.-H. Park, and B. I. Min, Importance of the van Hove singularity in superconducting $PdTe_2$, Phys. Rev. B **97**, 165102 (2018).

[9] M. Kang, S. Fang, J.-K. Kim, B. R. Ortiz, S. H. Ryu, J. Kim, J. Yoo, G. Sangiovanni, D. Di Sante, B.-G. Park, C. Jozwiak, A. Bostwick, E. Rotenberg, E. Kaxiras, S. D. Wilson, J.-H. Park, and R. Comin, Twofold van Hove singularity and origin of charge order in topological kagome superconductor CsV_3Sb_5, Nat. Phys. **18**, 301 (2022).

[10] Y. Sherkunov and J. J. Betouras, Electronic phases in twisted bilayer graphene at magic angles as a result of Van Hove singularities and interactions, Phys. Rev. B **98**, 205151 (2018).

[11] L. Classen, A. V. Chubukov, C. Honerkamp, and M. M. Scherer, Competing orders at higher-order Van Hove points, Phys. Rev. B **102**, 125141 (2020).

[12] H. Isobe, N. F. Q. Yuan, and L. Fu, Unconventional superconductivity and density waves in twisted bilayer graphene, Phys. Rev. X **8**, 041041 (2018).

[13] D. V. Efremov, A. Shtyk, A. W. Rost, C. Chamon, A. P. Mackenzie, and J. J. Betouras, Multicritical Fermi surface topological transitions, Phys. Rev. Lett. **123**, 207202 (2019).

[14] A. Shtyk, G. Goldstein, and C. Chamon, Electrons at the monkey saddle: A multicritical Lifshitz point, Phys. Rev. B **95**, 035137 (2017).

[15] I. M. Lifshitz, Anomalies of electron characteristics of a metal in the high pressure region, Zh. Eksp. Teor. Fiz. **38**, 1569 (1960) [Sov. Phys. JETP **11**, 1130 (1960)].

[16] C. Liu, T. Kondo, R. M. Fernandes, A. D. Palczewski, E. D. Mun, N. Ni, A. N. Thaler, A. Bostwick, E. Rotenberg, J. Schmalian, S. L. Bud'ko, P. C. Canfield, and A. Kaminski, Evidence for a Lifshitz transition in electron-doped iron arsenic superconductors at the onset of superconductivity, Nat. Phys. **6**, 419 (2010).

[17] A. I. Coldea, S. F. Blake, S. Kasahara, A. A. Haghighirad, M. D. Watson, W. Knafo, E. S. Choi, A. McCollam, P. Reiss, T. Yamashita *et al.*, Evolution of the low-temperature Fermi surface of superconducting $FeSe_{1-x}S_x$ across a nematic phase transition, npj Quantum Mater. **4**, 2 (2019).

[18] Y. Okamoto, A. Nishio, and Z. Hiroi, Discontinuous Lifshitz transition achieved by band-filling control in Na_xCoO_2, Phys. Rev. B **81**, 121102(R) (2010).

[19] E. A. Yelland, J. M. Barraclough, W. Wang, K. V. Kamenev, and A. D. Huxley, High-field superconductivity at an electronic topological transition in URhGe, Nat. Phys. **7**, 890 (2011).

[20] S. N. Khan and D. D. Johnson, Lifshitz transition and chemical instabilities in $Ba_{1-x}K_xFe_2As_2$ superconductors, Phys. Rev. Lett. **112**, 156401 (2014).

[21] S. Benhabib, A. Sacuto, M. Civelli, I. Paul, M. Cazayous, Y. Gallais, M.-A. Measson, R. D. Zhong, J. Schneeloch, G. D. Gu, D. Colson, and A. Forget, Collapse of the normal-state pseudogap at a Lifshitz transition in the $Bi_2Sr_2CaCu_2O_{8+x}$ cuprate superconductor, Phys. Rev. Lett. **114**, 147001 (2015).

[22] S. Slizovskiy, A. V. Chubukov, and J. J. Betouras, Magnetic fluctuations and specific heat in Na_xCoO_2 near a Lifshitz transition, Phys. Rev. Lett. **114**, 066403 (2015).

[23] D. Aoki, G. Seyfarth, A. Pourret, A. Gourgout, A. McCollam, J. A. N. Bruin, Y. Krupko, and I. Sheikin, Field-induced Lifshitz transition without metamagnetism in $CeIrIn_5$, Phys. Rev. Lett. **116**, 037202 (2016).

[24] Y. Sherkunov, A. V. Chubukov, and J. J. Betouras, Effects of Lifshitz transitions in ferromagnetic superconductors: The case of URhGe, Phys. Rev. Lett. **121**, 097001 (2018).

[25] M. E. Barber, F. Lechermann, S. V. Streltsov, S. L. Skornyakov, S. Ghosh, B. J. Ramshaw, N. Kikugawa, D. A. Sokolov, A. P. Mackenzie, C. W. Hicks, and I. I. Mazin, Role of correlations in determining the Van Hove strain in Sr_2RuO_4, Phys. Rev. B **100**, 245139 (2019).

[26] I. Stewart, Catastrophe theory in physics, Rep. Prog. Phys. **45**, 185 (1982).

[27] R. Markiewicz, B. Singh, C. Lane, and A. Bansil, Evolution of high-order van Hove singularities away from cuprate-like band dispersions and its implications for cuprate superconductivity, arXiv:2303.06520.

[28] F. Baumberger, N. J. C. Ingle, N. Kikugawa, M. A. Hossain, W. Meevasana, R. S. Perry, K. M. Shen, D. H. Lu, A. Damascelli, A. Rost, A. P. Mackenzie, Z. Hussain, and Z.-X. Shen, Nested Fermi surface and electronic instability in $Ca_3Ru_2O_7$, Phys. Rev. Lett. **96**, 107601 (2006).

[29] A. Steppke, L. Zhao, M. E. Barber, T. Scaffidi, F. Jerzembeck, H. Rosner, A. S. Gibbs, Y. Maeno, S. H. Simon, A. P. Mackenzie, and C. W. Hicks, Strong peak in Tc of Sr_2RuO_4 under uniaxial pressure, Science **355**, eaaf9398 (2017).

[30] M. E. Barber, A. S. Gibbs, Y. Maeno, A. P. Mackenzie, and C. W. Hicks, Resistivity in the vicinity of a Van Hove singularity: Sr_2RuO_4 under uniaxial pressure, Phys. Rev. Lett. **120**, 076602 (2018).

[31] N. F. Q. Yuan, H. Isobe, and L. Fu, Magic of high-order van Hove singularity, Nat. Commun. **10**, 5769 (2019).

[32] H. Isobe and L. Fu, Supermetal, Phys. Rev. Res. **1**, 033206 (2019).

[33] A. Chandrasekaran, A. Shtyk, J. J. Betouras, and C. Chamon, Catastrophe theory classification of Fermi surface topological transitions in two dimensions, Phys. Rev. Res. **2**, 013355 (2020).

[34] N. F. Q. Yuan and L. Fu, Classification of critical points in energy bands based on topology, scaling, and symmetry, Phys. Rev. B **101**, 125120 (2020).

[35] A. Chandrasekaran and J. J. Betouras, A practical method

to detect, analyze, and engineer higher order van Hove singularities in multi-band Hamiltonians, Adv. Phys. Res. **2**, 202200061 (2023).

[36] A. Chandrasekaran and J. J. Betouras, Effect of disorder on density of states and conductivity in higher-order Van Hove singularities in two-dimensional bands, Phys. Rev. B **105**, 075144 (2022).

[37] See Supplemental Material at http://link.aps.org/supplemental/10.1103/PhysRevResearch.5.L042006 for the details of the calculations and further results.

[38] A. V. Chubukov, D. V. Efremov, and I. Eremin, Magnetism, superconductivity, and pairing symmetry in iron-based superconductors, Phys. Rev. B **78**, 134512 (2008).

[39] R. Nandkishore, L. S. Levitov, and A. V. Chubukov, Chiral superconductivity from repulsive interactions in doped graphene, Nat. Phys. **8**, 158 (2012).

[40] S. Maiti and A. V. Chubukov, Renormalization group flow, competing phases, and the structure of superconducting gap in multiband models of iron-based superconductors, Phys. Rev. B **82**, 214515 (2010).

[41] Y.-P. Lin and R. M. Nandkishore, Parquet renormalization group analysis of weak-coupling instabilities with multiple high-order Van Hove points inside the Brillouin zone, Phys. Rev. B **102**, 245122 (2020).

[42] S. Maiti and A. V. Chubukov, Superconductivity from repulsive interaction, AIP Conf. Proc. **1550**, 3 (2013).

[43] As the electron-electron interactions are short ranged and under the assumption that the Wannier functions are not too extensive, the density-density interactions are expected to be of the same order as the exchange ones. In addition, the coupling constants will be significantly renormalized by two factors: (i) when excited bands as well as the states of the lowest bands outside the patches are integrated out, and (ii) by electron-phonon coupling. It is reasonable to integrate out the phonons to obtain phonon-mediated electron-electron effective interaction, which renormalizes the values of coupling constants. As a result it is possible to obtain exchange interactions larger than density-density ones.

[44] A. W. Rost, R. S. Perry, J. F. Mercure, A. P. Mackenzie, and S. A. Grigera, Entropy landscape of phase formation associated with quantum criticality in $Sr_3Ru_2O_7$, Science **325**, 1360 (2009).

[45] C. Lester, S. Ramos, R. S. Perry, T. P. Croft, R. I. Bewley, T. Guidi, P. Manuel, D. D. Khalyavin, E. M. Forgan, and S. M. Hayden, Field-tunable spin-density-wave phases in $Sr_3Ru_2O_7$, Nat. Mater. **14**, 373 (2015).

[46] V. Grinenko, S. Ghosh, R. Sarkar, J.-C. Orain, A. Nikitin, M. Elender, D. Das, Z. Guguchia, F. Brueckner, M. E. Barber, J. Park, N. Kikugawa, D. A. Sokolov, J. S. Bobowski, T. Miyoshi, Y. Maeno, A. P. Mackenzie, H. Luetkens, C. W. Hicks, and H.-H. Klauss, Split superconducting and time-reversal symmetry-breaking transitions in Sr_2RuO_4 under stress, Nat. Phys. **17**, 748 (2021).

[47] Y.-S. Li, M. Garst, J. Schmalian, S. Ghosh, N. Kikugawa, D. A. Sokolov, C. W. Hicks, F. Jerzembeck, M. S. Ikeda, Z. Hu, B. J. Ramshaw, A. W. Rost, M. Nicklas, and A. P. Mackenzie, Elastocaloric determination of the phase diagram of Sr_2RuO_4, Nature (London) **607**, 276 (2022).

[48] J. Yang, W. Wang, Y. Liu, H. Du, W. Ning, G. Zheng, C. Jin, Y. Han, N. Wang, Z. Yang, M. Tian, and Y. Zhang, Thickness dependence of the charge-density-wave transition temperature in VSe_2, Appl. Phys. Lett. **105**, 063109 (2014).

[49] M. J. Trott and C. Hooley, A potential all-electronic route to the charge-density-wave phase in monolayer vanadium diselenide, Commun. Phys. **4**, 37 (2021).

[50] J. Feng, D. Biswas, A. Rajan, M. D. Watson, F. Mazzola, O. J. Clark, K. Underwood, I. Markovic, M. McLaren, A. Hunter, D. M. Burn, L. B. Duffy, S. Barua, G. Balakrishnan, F. Bertran, P. Le Fvre, T. K. Kim, G. van der Laan, T. Hesjedal, P. Wahl *et al.*, Electronic structure and enhanced charge-density wave order of monolayer VSe_2, Nano Lett. **18**, 4493 (2018).

[51] M. Esters, R. G. Hennig, and D. C. Johnson, Dynamic instabilities in strongly correlated VSe_2 monolayers and bilayers, Phys. Rev. B **96**, 235147 (2017).